Renewable Energy 186 (2022) 535–546

Contents lists available at ScienceDirect

Renewable Energy

journal homepage: www.elsevier.com/locate/renene

# Non-conventional tube shapes for lifetime extend of solar external receivers

M.R. Rodríguez-Sánchez [a, *], M. Laporte-Azcué [a], A. Montoya [b], F. Hernández-Jiménez [a]

[a] Energy Systems Engineering Group (ISE), Department of Thermal and Fluid Engineering, University Carlos III of Madrid, Av. Universidad 30, 28911, Leganés, Spain
[b] Continuum Mechanics and Structural Analysis Department, University Carlos III of Madrid, Av. Universidad 30, 28911, Leganés, Spain

ARTICLE INFO

*Article history:*
Received 17 September 2021
Received in revised form
17 December 2021
Accepted 5 January 2022
Available online 12 January 2022

*Keywords:*
Tubular solar receiver
Mechanical model
Thermal model
Asymmetric geometry

ABSTRACT

In this work, several novel tube shapes of solar tubular receivers that differ from the classical circular shape are analysed aiming to reduce the stresses of the receiver tubes, without penalizing its thermal efficiency. The analysis is performed using analytical thermal and mechanical models of the literature adapted for their use with non-circular tube shapes, verifying the assumptions made with FEM simulations due to the lack of experimental data available.

Among the geometries studied, the results show that oval cross-section tubes improve the thermal efficiency of the receiver at the expense of increasing the stresses considerably. Ovoidal tubes show worse thermal and mechanical behaviour when the frontal part becomes peakier. Semicircle tubes reduce the stress by 10.9%, while keeping constant or even slightly improving the thermal performance. The last ones, increase the lifetime of the receiver and reduces the receiver costs if the manufacturing of the new geometries does no overpass 3.5 times the present price of production of the circular tubes. Therefore, the use of asymmetric cross-section tubes with low rear-front surface ratios, and smooth front surfaces can be considered a good alternative for substituting traditional circular cross-section tubes in central receivers.



## 1. Introduction

42% of the solar power tower (SPT) issues are related to the receiver system [1], where maintenance and operation represent an important percentage of the SPT costs. The main failure mechanism in the solar receiver tubes is the appearance of cracks due to thermal stresses, cyclic fatigue, and creep. The important role of the tube temperature in the correct plant operation makes it essential to improve their performance and solve the issues that cause the receiver early failure.

Numerous authors tried to optimize the receiver design to improve their reliability. Among the designs proposed, here are outlined those that try to maximize the absorbed heat flux by modifying the structure of the receiver, opposite to the cylindrical one: pyramidal receivers [2], star-shaped or with fins [3]; those that proposed new tube material and heat transfer fluids (HTFs) to reduce the corrosion and increase the operation temperature [4,5]; and those with the goal of homogenising the receiver tube wall temperature [6] or increasing the receiver thermal efficiency and reliability [7,8]. The latter follows two different paths: on the one hand, the modification of the receiver configuration by varying the tube diameter within a panel [9], by installing valves that allow the modification of the fluid velocity along the receiver [10], or by proposing different flow paths configurations [11]; on the other hand, the modification of the tube geometry using corrugated tubes [12], or eccentric bayonet tubes [13]. However, most of those studies have been carried out from a thermal point of view without considering the influence of the new designs on the stress distribution or on the receiver lifetime.

As the experimental data related to central receivers is limited in the literature, the development of models is vital for understanding the behaviour of these systems. Therefore, accurate modelling of such systems is a key factor in the evolution of the technology and during their operation lifetime. In this regard, more detailed simulations can be employed, like FEM or CFD, but also simplified

*Abbreviations:* AM, Additive manufacturing.; CFD, Computational fluid dynamics.; CGM, Coarse grid model.; EODs, equivalent operating days.; FEM, Finite element model.; GPS, Generalized plane strain.; HTF, Heat transfer fluid.; SPT, Solar power tower.

* Corresponding author.
*E-mail address:* mrrsanch@ing.uc3m.es (M.R. Rodríguez-Sánchez).

https://doi.org/10.1016/j.renene.2022.01.015

**Nomenclature**

| | |
|---|---|
| $A$ | Area ($m^2$) |
| $C$ | Cost ($) |
| $C_p$ | Specific heat at constant pressure (J/kgK) |
| $D$ | Receiver diameter (m) |
| $Diff$ | Difference (%) |
| $d$ | Tube diameter (m) |
| $E$ | Young modulus (Pa) |
| $E_{rr}$ | Error (%) |
| $F$ | View factors |
| $f$ | Correction factor |
| $Gr$ | Grashof number |
| $H$ | Receiver and tube length (m) |
| $h$ | Convective coefficient ($W/m^2K$) |
| $k$ | Thermal conductivity (W/mK) |
| $N$ | Number of elements |
| $n$ | Number of circumferential divisions in the tubes |
| $n+1$ | Receiver frame |
| $p$ | Perimeter (m) |
| $Pr$ | Prandtl number |
| $Q$ | Heat power absorbed by the tubes (W) |
| $q$ | Heat flux ($W/m^2$) |
| $Re$ | Reynolds number |
| $T$ | Temperature (K) |
| $t$ | Time (h) |
| $th$ | Thickness (m) |
| $V$ | Volume ($m^3$) |
| $\Delta_Z$ | Length of each axial division (m) |
| 0 | Surroundings |

Greek symbols

| | |
|---|---|
| $\alpha$ | Absorptivity of the solar radiation in the visible spectrum |
| $\delta$ | Kronecker delta |
| $\varepsilon$ | Emisivity |
| $\lambda$ | Linear dilatation coefficient ($K^{-1}$) |
| $\rho$ | Density ($kg/m^3$) |
| $\sigma$ | Stress (Pa) |
| $\boldsymbol{\sigma_B}$ | Stefan-Boltzmann constant ($W/m^2K^4$) |
| $\boldsymbol{\nu}$ | Poisson coefficient |

Subscripts

| | |
|---|---|
| $a$ | Allowable |
| $amb$ | Ambient |
| $bp$ | Black Pyromark |
| $c$ | Creep. Crown |
| $cp$ | Clips |
| $eq$ | Von Mises equivalent stress |
| $f$ | Fatigue |
| $fc$ | Forced convection |
| $hd$ | Headers |
| $hel$ | Heliostats |
| $i$ | Inner |
| $in$ | Inlet. |
| $m$ | Mean |
| $max$ | Maximum |
| $nc$ | Natural convection |
| $nz$ | Nozzle |
| $o$ | Outer |
| $p$ | Panels |
| $R$ | Rupture |
| $rep$ | Replacement |
| $rp$ | Repaint |
| $t$ | Tubes |
| $th$ | Thermal |

models can be very helpful. The advantages of the simplified models mainly consist in that they are easy to implement, and their calculation speed up, which makes CFD and FEM simulations unfeasible for the calculation of the whole receiver. However, they must be validated or verified. Validated against experimental data if available and verified against more detailed models like in the present work.

The main goal of this work is to analyse different tube geometries (circular, oval, ovoid and semicircle) to be used in tubular SPT receivers by means of coupled thermal and mechanical models. The new tube designs proposed are asymmetrical, trying to homogenise the wall temperature of the tubes to reduce the stresses without penalizing the thermal efficiency of the receiver. In this way the creep-fatigue damage of the receiver, which depend both on the temperature and equivalent stress level [14], will be reduced assuring the receiver lifetime and decreasing the maintenance cost of the SPT.

## 2. Thermal and mechanical models

To analyse the proposed tube geometries for external solar receivers, several analytical models have been employed to carry out the optical study of the solar field, as well as the thermal and mechanical characterization of the receiver.

The solar flux distribution on the receiver surface is obtained with the convolution projection stand-alone free software tool FluxSPT[1] [15], which was validated using experimental data of "Plataforma Solar de Almería" and Thèmis and using Monte Carlo ray tracing methods obtaining good agreement [16,17]. As the input data, this model needs the solar field layout, the location, the ambient conditions, the tower height, and the receiver length ($H$), diameter ($D$) and number of panels ($N_p$). Then, the solar flux distribution feeds the analytical 2D thermal Coarse Grid Model (CGM), developed in Ref. [18] and verified with detailed computational fluid dynamics (CFD) simulations [19]. The CGM obtains the heat exchanged and the temperature profile on a representative tube of each receiver panel, considering that all the tubes of a panel work at the same conditions. This model assumes circumferential variations of the heat flux distribution on the tube surface, considering radiative heat exchange between the tubes, the receiver frame, and the sky. For an axial section of tube, the heat power absorbed by the HTF is calculated as follows,

$$Q_t = \sum_{j=1}^{n} q_j p_j \Delta z - \sum_{j=1}^{n} \overline{h}_o p_j \Delta z (T_{t,j} - T_{amb}) \quad (1)$$

where the first term of the equation corresponds to the heat transferred to the tube after the radiative heat exchange, being $q$ the net heat flux for each $n$ circumferential division of tube calculated with Eq. (2). Here, the value $m = 0$ corresponds to the surroundings, $m = n + 1$ represents the receiver frame and the rest of values for $m$ are the $n$ circumferential cells in which an axial

[1] http://ise.uc3m.es/research/solar-energy/fluxspt/

division of tube is discretized, see Fig. 1. $F$ corresponds to the 2D view factors matrix among the $m$ surfaces considered. Those geometrical factors are calculated using the crossed-string method [20]. The error committed using 2D view factors is acceptable when the axial number of divisions in which the tube is discretized is higher than once the tube diameter.

The different surfaces have been considered grey and diffuse, allowing to calculate the radiative heat transfer by balancing the outgoing radiation travelling directly from surface to surface. In the first step of the calculation it is estimated and in following iterations it is recalculated.

$$m = 0, \ldots, n+1$$

$$\sum_{j=0}^{n}\left[\frac{\delta_{m,j}}{\varepsilon_j} - \left(\frac{1}{\varepsilon_j} - 1\right)F_{m,j}\right]\frac{q_j}{\sigma_B} - \left[\delta_{m,n+1} - F_{m,n+1}\right]T_{n+1}^4 = \sum_{j=0}^{n}\left[\delta_{m,j} - F_{m,j}\right]T_j^4 - \left[\frac{\delta_{m,n+1}}{\varepsilon_{n+1}} - \left(\frac{1}{\varepsilon_{n+1}} - 1\right)F_{m,n+1}\right]\frac{q_{n+1}}{\sigma_B} - F_{m,0}\frac{q_{hel}}{\sigma_B}\alpha \tag{2}$$

The second term of Eq. (1) corresponds to the heat losses of external convection, considering both natural and forced convection as follows:

$$\overline{h}_o = \left(\overline{h}_{fc}^{\,3.2} + \overline{h}_{nc}^{\,3.2}\right)^{\frac{1}{3.2}} \tag{3}$$

$$\overline{h}_{fc} = \frac{k_{air}}{D}\left\{0.3 + 0.488Re_D^{0.5}\left[\left(1 + \left(\frac{Re_D}{282000}\right)^{0.625}\right)1 + \left(\frac{Re_D}{282000}\right)^{0.625}\right]^{0.8}\right\} \tag{4}$$

$$\overline{h}_{nc} = \frac{k_{air}}{H}0.098Gr_H^{\frac{1}{3}}\left(\frac{\overline{T}_t}{T_{amb}}\right) \tag{5}$$

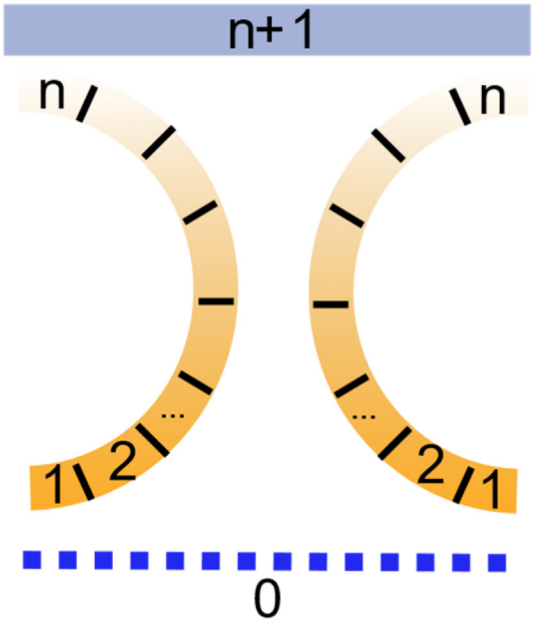


**Fig. 1.** Schematic of calculation.

where the forced convection is based on the receiver diameter considering cross flow around a cylinder in which the tubes represent the roughness of the cylindrical heat exchanger. Once the heat flux absorbed by the tubes is known, it is possible to recalculate the tube external wall temperature and the radiative heat losses:

$$T_t = T_{HTF,in} + \frac{\sum_{j=1}^{n} q_j p_j}{\dot{m}C_p}z + \frac{q_t}{\left(\frac{1}{h_i}\frac{d_o}{d_i} + \frac{d_o \ln\left(\frac{d_o}{d_i}\right)}{2k_t}\right)^{-1}} \tag{6}$$

Here, $h_i$ is calculated using Gnielinski correlation for internal flow. During the iterative process $\dot{m}$ is modified after calculating a whole flow path if the $T_{HTF}$ at the exit of the receiver is different to a set temperature (565 °C, detailed in Section 3).

The following assumptions have been considered to adapt the CGM to the proposed new tube geometries analysed in this study:

- the view factors for radiative heat transfer calculations will change in agreement with the new geometries,
- the external convective calculations remain constant, although the relative roughness of the receiver changes depending on the tube geometry and size,
- Gnielinski equation can still be used for the internal convection, modifying the Reynolds number and the Darcy factor as a function of the hydraulic diameter.

To calculate the stress on the receiver tubes, both the temperature profile and the external mechanical supports of the tubes are considered. Usually, receiver tubes are periodically guided with supports, called clips, that allow them longitudinal enlargement but limit the tube displacement in the cross-section plane to avoid contact between adjacent tubes and excessive bending. As a first approximation to study the feasibility of the new geometries proposed, a simplified one-dimensional approach introduced by Ref. [21] has been used to calculate the equivalent stress on the tube crown (part of the tube exposed to the heliostat field, in which the maximum stresses are located). This methodology is ideal to study asymmetrical tube geometries in a simple way because it does not require the effect of the tube size, the cross-sectional shape, or the wall thickness.

$$\sigma_{eq,c} = \lambda E\left[\left(\frac{T_{c,o} + T_{c,i}}{2} - T_{HTF} - \frac{1}{\pi}\left(T_{m,c} - T_{HTF}\right)\right) + \left(\frac{T_{c,o} - T_{c,i}}{2(1-\nu)}\right)\right] \tag{7}$$

To obtain the complete stress profile of the receiver tubes and the equivalent von Mises stress with moderately low computational cost, the 2D model developed in Ref. [22] has been used for the reference circular cross-section tube geometry. This model is fed with the temperature distribution on the receiver tubes, considers temperature dependence of mechanical properties and uses the generalized plane strain (GPS) approximation to regard the external boundary conditions [23]. It allows to obtain the different components of the stress in the entire tube, not only in the crown:

$$\sigma_{eq}^E = \sqrt{\frac{(\sigma_r - \sigma_\theta)^2 + (\sigma_\theta - \sigma_z)^2 + (\sigma_z - \sigma_r)^2}{2} + 3\tau_{r\theta}{}^2} \tag{8}$$

where $\sigma_r$ and $\sigma_\theta$ only depend on the temperature distribution. They are calculated after the decomposition of the temperature profile into a geometrical average (axisymmetric) and circumferentially

varying (non-axisymmetric and non-uniform) parts.

$$T_\theta = T_t - T_r = T_t - (\overline{T_i} - \overline{T_o})\frac{\ln\left(\frac{d_o}{2r}\right)}{\ln\left(\frac{d_o}{d_i}\right)} - \overline{T_o} \tag{9}$$

The last temperature can be expressed as a plane harmonic Fourier series with radial dependent functions, allowing express the stress components as follows:

$$\sigma_r = \frac{r}{\left(\frac{d_i}{2}\right)^2 + \left(\frac{d_o}{2}\right)^2}(B_1 cos\theta + D_1 sin\theta)\frac{\lambda E}{2(1-\nu)}\left(1 - \frac{\left(\frac{d_i}{2}\right)^2}{r^2}\right) \times \left(1 - \frac{\left(\frac{d_o}{2}\right)^2}{r^2}\right) + \frac{E}{1-\nu}\left[\left(1 - \frac{\left(\frac{d_i}{2}\right)^2}{r^2}\right)\frac{1}{2}\overline{\lambda T} - \frac{1}{r^2}\int_a^r \lambda_r T_r\, r\, dr\right] \tag{10}$$

$$\sigma_\theta = \frac{r}{\left(\frac{d_i}{2}\right)^2 + \left(\frac{d_o}{2}\right)^2}(B_1 cos\theta + D_1 sin\theta)\frac{\lambda E}{2(1-\nu)}\left(3 - \frac{\left(\frac{d_i}{2}\right)^2 + \left(\frac{d_o}{2}\right)^2}{r^2} - \frac{\left(\frac{d_i}{2}\right)^2\left(\frac{d_o}{2}\right)^2}{r^4}\right) + \frac{E}{1-\nu}\left[\left(1 + \frac{\left(\frac{d_i}{2}\right)^2}{r^2}\right)\frac{1}{2}\overline{\lambda T} + \frac{1}{r^2}\int_a^r \lambda_r T_r\, r\, dr - \lambda_r T_r\right] \tag{11}$$

$$\tau_{r\theta} = \frac{r}{\left(\frac{d_i}{2}\right)^2 + \left(\frac{d_o}{2}\right)^2}(B_1 sin\theta - D_1 cos\theta)\frac{\lambda E}{2(1-\nu)}\left(1 - \frac{\left(\frac{d_i}{2}\right)^2}{r^2}\right) \times \left(1 - \frac{\left(\frac{d_o}{2}\right)^2}{r^2}\right) \tag{12}$$

Note that to avoid excessive complexity, the previous expressions were obtained assuming properties independent of the temperature, although to solve the problem the dependence of the properties with the temperature is considered.

On the other hand, the axial stress $\sigma_z$ depends on the temperature distribution but also on the mechanical boundary conditions, GPS in this case.

$$\sigma_z = \nu(\sigma_r + \sigma_\theta) - \lambda E T + \frac{E}{E_0}\frac{\int_A \lambda E T\, dA}{\int_A (E/E_0)\, dA} \tag{13}$$

The stress calculation in the tube cross-section becomes extremely laborious when applied to non-circular cross-section tubes. Therefore, to study the proposed new tube geometries, a simplification based on circular cross-section tubes whose diameter is the corresponding hydraulic diameter of the geometry but considering the real tube temperature adapted to the circular shape, has been applied to the 2D methodology. To test the validity of this simplification to the new tube geometries proposed in this work, verifications have been carried out for a representative cross-section of each new proposed configuration using a Finite Element Model (FEM) implemented in the software Abaqus/Standard. This FEM has been also used to quantify the error committed using the 1D simplified methodology in the characterization of the different tube geometries.

The FEM analysis is carried out using a 2D GPS methodology for the whole tube. The discretization has been made with 4-node linear quadrilateral elements for GPS analysis (CPEG4T in Abaqus). Before carrying out the analysis of this work, FEM has been validated using a case whose analytical solution is well-known: a long circular cylinder heated axisymmetrically, with an uniform temperature difference between internal and external radii of 20 °C, in generalized plane strain state (case 135 from Ref. [24]. Results from the analytical equations and the FEM model are compared in Fig. 2 a, seeing that the results match in every stress component. Besides, a the sensibility analysis is shown in Fig. 2 b, as a compromise between computational cost and accuracy, the model has been meshed with 40 elements along the thickness with an aspect ratio of 1, for all the geometries studied. Internal and external tube wall temperatures from the thermal model are imported as boundary conditions for the FEM.

## 3. Geometries of study

The solar field layout and the receiver and tower dimensions remain the same for all the receiver tube geometries studied. The HTF used is solar salt, whose properties are detailed in Ref. [25]. The inlet temperature of the HTF in the receiver is 290 °C and the outlet set temperature is 565 °C. The solar flux distribution on the receiver surface is also the same for all the cases analysed, which corresponds to the solar noon of the spring equinox in Seville, Spain, using a circular solar field like Gemasolar [26], composed by 6500 heliostats, each of them with a surface of 120 $m^2$ and using a flat aiming strategy.

The receiver is located at the top of a 120 m tower, and it has an effective length ($H$) of 10.5 m and 8.5 m of diameter ($D$). It is compound of 18 panels, divided in two symmetrical flow paths with the inlet in the northern face and the outlet in the southern one, see Fig. 3. The tubes are made of Inconel 625, a nickel based alloy usually employed in solar receivers. By their outer surface, tubes are coated with black Pyromark to improve the optical behaviour of the tubes. Properties of both materials have been obtained from Refs. [27,28], respectively. The reference circular tubes have an external diameter ($d_o$) of 2.2 cm and a thickness ($th$) of 1.65 mm.

Regarding the new tube geometries, from the examination of the aforementioned models [18,22] it can be concluded that the stresses could diminish if the tube crown temperature decreases or if the mean tube temperature increases. This could be obtained by flattening the tube surface in the front side of the tubes or reducing the rear surface ratio with respect to the frontal one. Trying to fulfil those considerations, the behaviour of oval and ovoid cross-section tubes for the working conditions specified has been studied. All the selected geometries are formed by circular arcs to allow the calculation of the view factors and they have smooth transitions from rear to front sides to avoid pressure stresses on the possible corners.

The new tube geometries studied have the goal of having: *i)* the same projected surface to keep the number of tubes in a panel and

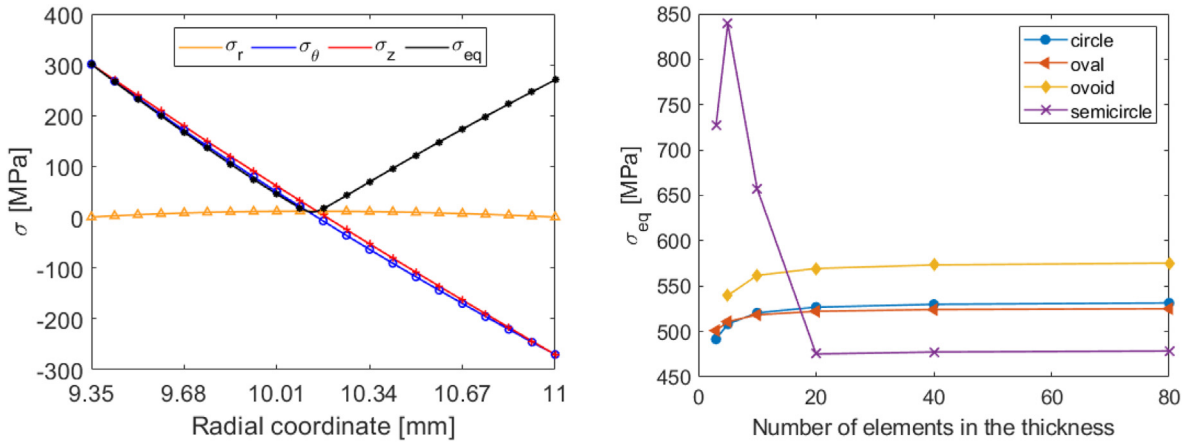


**Fig. 2.** a) Stress components along the thickness for a tube axisymmetrically heated in GPS state. Solid lines denote analytical results from Ref. [24], and markers denote results from 2D FEM model. b)Sensitivity analysis of the FEM mesh for the different geometries analysed.

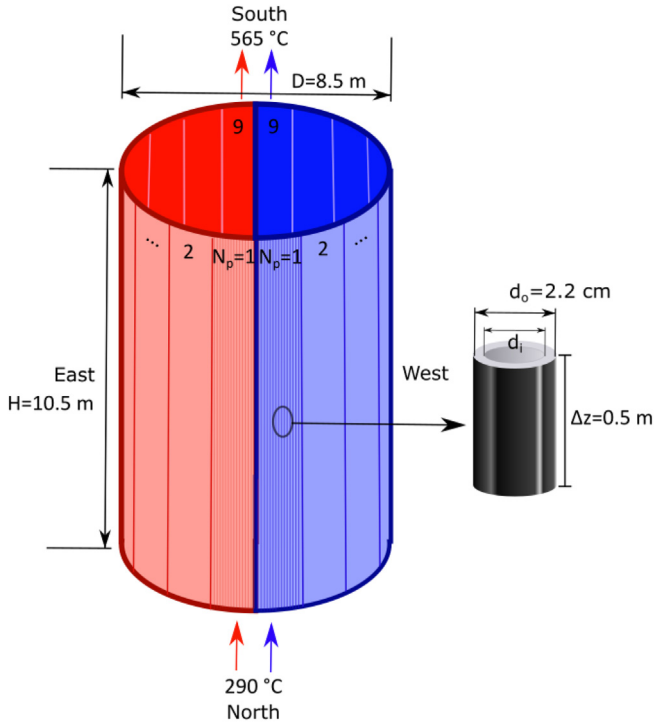


**Fig. 3.** Schematic of the receiver and detail of a diferential element of tube.

the effective area of absorption, and *ii)* the same cross-section. In cases in which both conditions could not be fulfilled, one of the following actions have been executed: to slightly modify the projected area, increasing or reducing the tube separation to keep constant the number of tubes in the receiver panels; or to double both the projected and the cross-section areas with respect to the reference receiver tubes, reducing the number of tubes per panel by half. The mass flow rate in each configuration varies with respect to the reference case depending on the receiver thermal efficiency to reach the set outlet temperature.

## 4. Results

The calculation of thermal stresses in circular cylinders with a non-uniform temperature distribution has been widely studied in the literature and analytical solutions have been developed. In this research, since some simplifications has been made in the analytical models to try to approximate the results for the non-circular cross-sections tubes, the numerical simulations are used as a benchmark for both 1D and 2D analytical models to check the validity of their solutions. After that, a scan of the different geometries proposed has been carried out to search the optimum receiver tube design able to reduce the stresses without diminishing the thermal efficiency.

### 4.1. Mechanical models verification

All the models have been fed with the temperature profile obtained with the 2D thermal model. The results obtained are summarised in Table 1, where the results of the maximum equivalent stress for the axial division with the greatest stress are presented for the different geometries tested. The deviation between the analytical models and the FEM simulations is also included in the Table 1.

The 1D methodology results in a consistent underestimation of the stress (~10%) at the tube crown for the different geometries with respect to the FEM outcome. This difference is high enough to overestimate the receiver lifetime, which could result in the unpredicted premature receiver failure that could be disastrous for the SPT operation and its economic viability. However, it could be used for a first estimation when comparing different tube geometries.

Table 1 is combined with Fig. 4 (circular), 5 (oval), 6 (ovoid) and 7 (semicircle) where the temperature and equivalent stress profiles in the most problematic axial division obtained with the thermal model and FEM, respectively, are presented. Besides the stress relative deviation between the FEM and the 2D methodology is shown. In the figures, the maximum value of each variable is also included. The maximum temperature and stress is at the external wall of tube crown, facing the heliostat field. The minimum temperature is at the rear half of the tube, while the minimum stress is at the sides of the tubes, slightly displaced to the tube crown where the temperature gradient is minimum.

In view of Fig. 4, the relative error is maximum at the sides of the tube where the stress gradient is high due to the temperature passes from its maximum to its minimum. Yet, this error is lower than 5%. In zones with higher stress, this error decreases under 1%. Then, the 2D methodology can be used to accurately predict the stresses in circular cross-section tubes.

**Table 1**
Summary of the maximum equivalent stress results.

| CASE | FEM (MPa) | 1D (MPa) | 1D deviation from FEM (%) | 2D (MPa) | 2D deviation from FEM (%) |
|---|---|---|---|---|---|
| **Circular** | 529.97 | 476.6 | 10.07 | 531.2 | −0.23 |
| **Oval** | 524.19 | 477.1 | 8.98 | 517.54 | 1.26 |
| **Ovoid** | 573.39 | 506.7 | 11.63 | 572.98 | 0.07 |
| **Semicircle** | 477.52 | 424.4 | 11.12 | 456.12 | 4.48 |

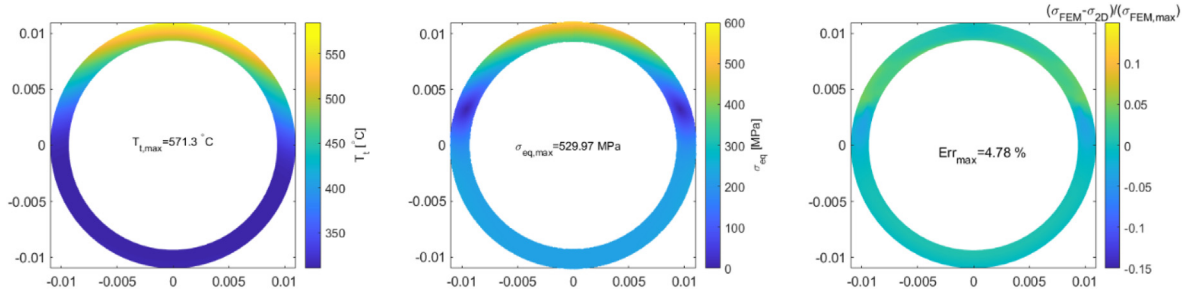


**Fig. 4.** a) Temperature profile, b)FEM equivalent stress and, c) error committed between the FEM and the 2D methodology in the most problematic axial division of a circular cross-section tube.

For an arbitrary oval tube cross-section (Fig. 5), the maximum temperature is almost the same, but the stress is slightly lower than for the case of a circular cross-section tube, being the distribution of the temperature and stresses quite like the reference case. The 2D methodology overestimates the crown stress in only 0.1% with respect to FEM, with a maximum error of 12.9% at the sides of the tube where the transitions between circular sections are located and the stress is minimum.

Regarding a random ovoidal cross-section receiver tube (Fig. 6), the maximum temperature and stress increases with respect to the reference tube geometry in more than 11 °C and 40 MPa, respectively. The approximation used to solve the stresses of the different tube geometries with the 2D methodology gives an error of less than 0.1% in the tube crown with respect to FEM. However, the difference increases up to 6.33% in the lateral sides of the ovoidal tube, where the transitions between circular sections are located. Nevertheless, at these spots, the stresses are low enough to assure not permanent damage in the receiver tubes.

Finally, for the semicircle cross-section tubes (Fig. 7), in which the cross-section area is twice the reference circular tube one, the maximum temperature raises 15 °C, but the stress calculated with FEM decreases more than 50 MPa with respect to the reference circular cross-section, with similar distribution along the tube walls. The 2D methodology using the hydraulic diameter increases the error up to 14.8% at the transition spot between the different circles that compose the entire figure, where the stresses are low, but the error is lower than 5% in the tube crown.

### 4.2. Geometry optimisation

The procedure followed consists in scanning different cases for each tube geometry using the low computational cost 1D model. Once that the optimum case for each geometry is selected, the FEM model is employed for validation purposes. Finally, the behaviour of the optimum geometry, selected for substituting the reference circular tubes, is studied for the whole receiver using the 2D analytical model, to ensure that the geometry does not penalize other axial sections of the receiver. For the optimum geometry, a lifetime and cost analysis are carried out to check the feasibility of using it instead of the circular reference tubes. It is worth noting that among the different geometries tested, the thermal efficiency of the receiver is affected by multiple factors such as the internal convection coefficient, the heat transfer area, the distance between tubes or the view factors.

#### 4.2.1. Ovals

14 different frontal ovals with the peaky side facing the solar field are studied, see Fig. 8. The main axis of the oval goes from $1.1d_o$ to $1.7d_o$ in increments of 1 mm while keeping constant the cross-section, being $d_o$ the outer diameter of the reference circular tube equal to 2.2 cm. The peak of the oval increases as well as the space between tubes to keep constant the number of tubes in the

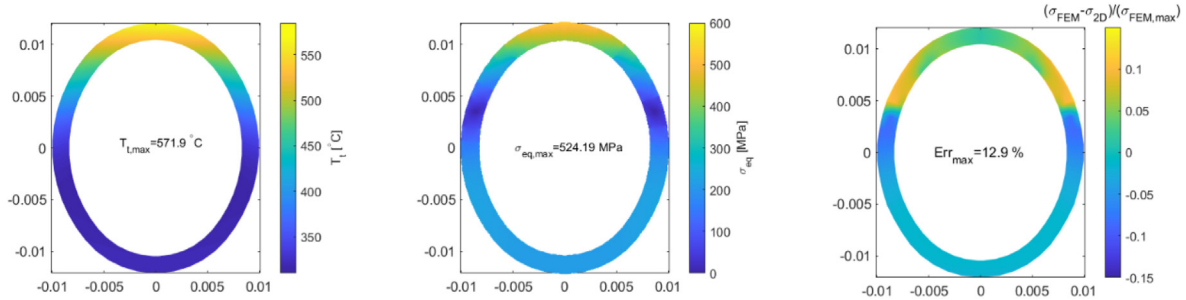


**Fig. 5.** a) Temperature profile, b) FEM equivalent stress and, c) Error committed between the FEM and the 2D methodology in the most problematic axial division of an oval cross-section tube.

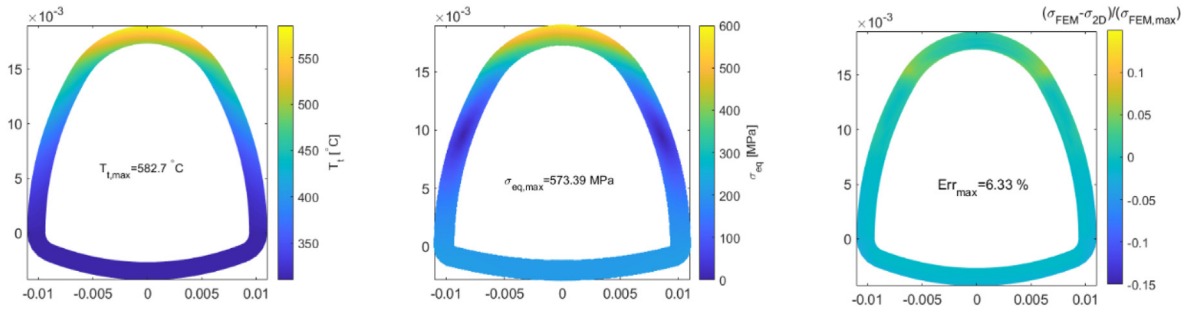


**Fig. 6.** a) Temperature profile, b) FEM equivalent stress and, c) error committed between the FEM and the 2D methodology in the most problematic axial division of an ovoidal cross-section tube.

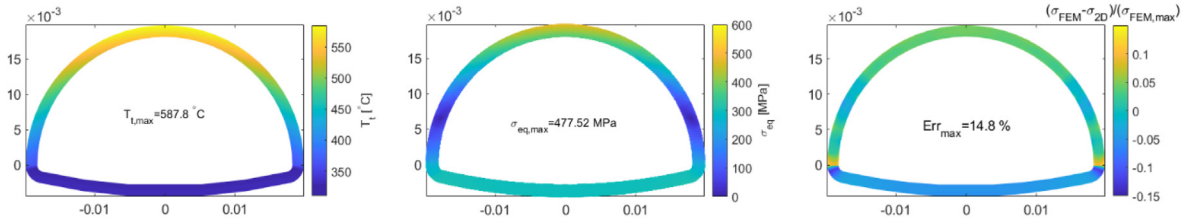


**Fig. 7.** a) Temperature profile, b) FEM equivalent stress and, c) error committed between the FEM and the 2D methodology in the most problematic axial division of a semicircle cross-section tube.

receiver. Thus, the effective absorber area of the receiver decreases.

Fig. 9 shows the maximum tube wall temperature, the mean tube temperature, the crown equivalent von Mises stress, and the thermal efficiency for the reference circular tube ($d_o$ case) and the 14 frontal oval tubes resulting from the main axis variation, at the axial division with the highest stress. The maximum tube temperature, located at the tube crown, increases from 569.2 °C in the circular tube to 626.2 °C as the oval geometry becomes peakier. After case $1.33d_o$ a discontinuity in the evolution of the different variables is seen, attributed to the sharpened shape of the oval and the higher gap between tubes, that produces a change in the tangent position between two adjacent tubes. It modifies the view factors configuration, increasing the incident solar flux in the rear half of the receiver tubes.

The mean temperature in the tube perimeter remains almost constant until case $1.33d_o$, in which the tubes are almost circular, and suffers an important decrement for the following sharpened cases. All this entails an increment of the thermal stresses from 476.6 MPa for the circular case to 641.5 MPa in the most sharpened oval, with intermediate values in soft ovals. The stresses are highly influenced by the crown temperature. Ovals also present an increment of the receiver thermal efficiency, from 78.9% to 82.9%. Therefore, oval tubes from thermal point of view improve the performances, but behave worse regarding the stresses and receiver lifetime when peaky ovals are employed.

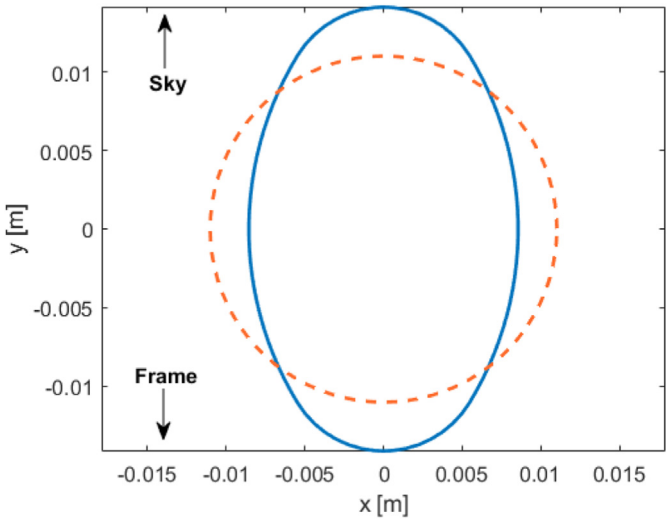


**Fig. 8.** Example of a frontal oval cross-section compared to the reference circular tube.

### 4.2.2. Ovoids

To minimize the rear area of the tubes to increase the mean temperature of the cross-section and, in this way, reduce the stresses, ovoidal cross-section tubes are studied. They are formed by two semiovals, one frontal and another tilted, to avoid pressure stresses in the corners between the straight zone (rear) and the frontal one, see Fig. 10. Both the projected and the cross-section areas are kept constant with respect to the reference circular tube. To achieve that having fixed the minor axis, equal to $d_o$, the major axis varies from a circular configuration to one in which the major axis is $2d_o$ in increments of 1 mm, with a total of 24 different geometries analysed. In this scan, the frontal half area of the tubes increases at the expense of the rear half area.

Fig. 11 shows the maximum wall temperature, the mean tube temperature, the crown equivalent von Mises stress, and the thermal efficiency for the 24 cases analysed, in which the first case ($d_o$) corresponds to the reference circular cross-section tube. The temperatures and the stresses suffer several trend changes: from cases $1.04d_o$ to $1.13d_o$, in which the asymmetry is small, the maximum temperature and the stresses decrease slightly to then increase from case $1.18d_o$ onwards, reaching a maximum stress of 538.7 MPa, increasing more than 60 MPa with respect to the reference case. From the thermal point of view, these geometries slightly improve the efficiency of the receiver, from 78.9% to 80.1%.

Finally, to keep the circular shape in the front part of the tubes and to avoid increasing the peak as in previous case, ovoidal

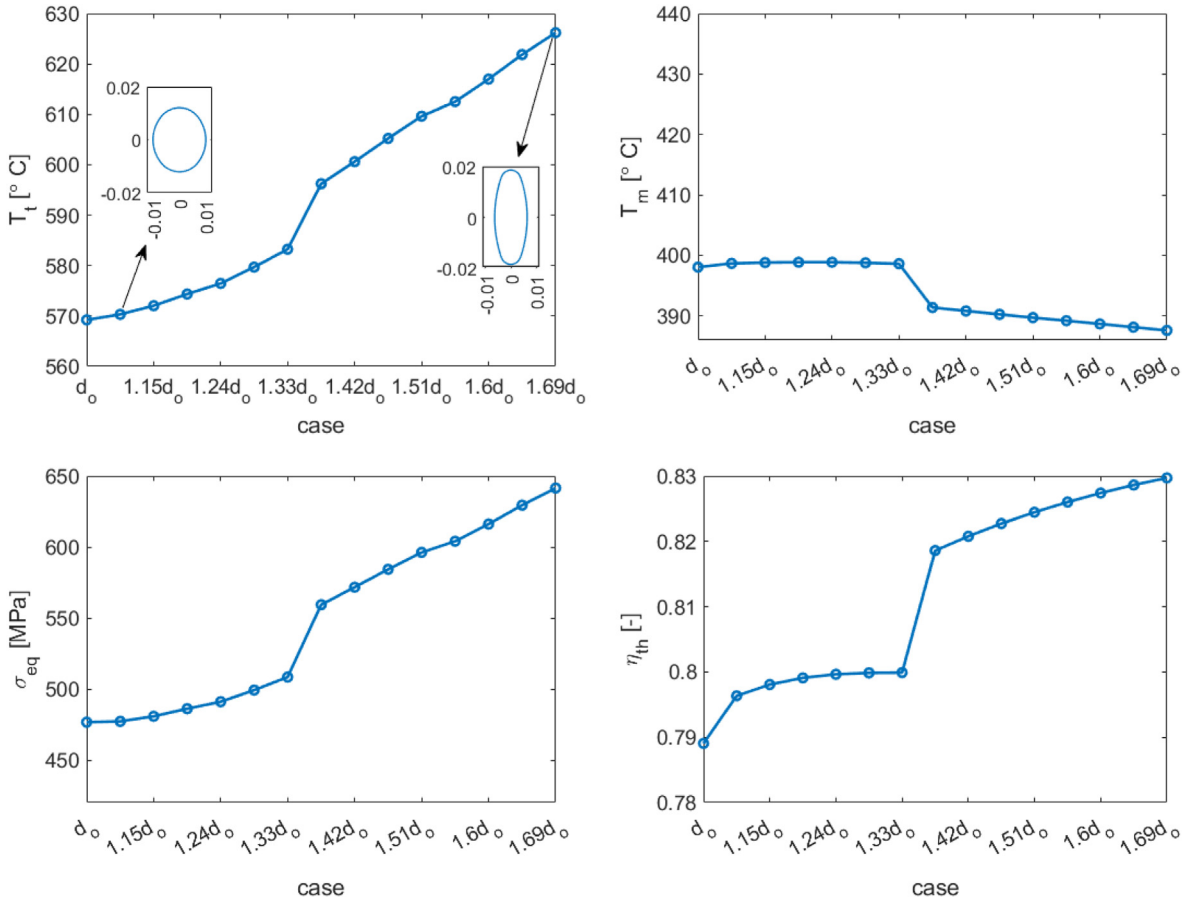


**Fig. 9.** Oval cross-section tube results for the a) maximum tube wall, b) mean temperature of the tubes c) equivalent von Misses stress and d) thermal efficiency of the receiver for the most problematic axial division.

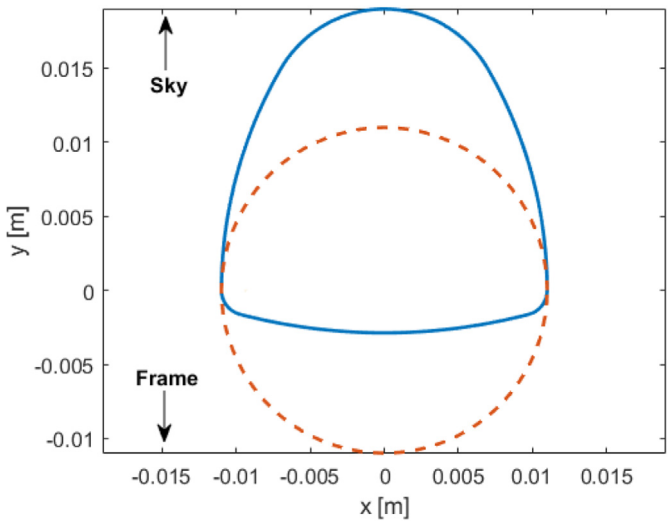


**Fig. 10.** Ovoidal cross-section compared to the reference circular tube.

configurations like semicircles shaped tubes have been studied. In this configuration the ovoid is formed by a semicircle in the front part and a tilted semioval in the rear one, doubling the reference circular tube cross-section and the separation between tubes, see Fig. 12. A scan in which the projected area is slightly reduced with respect to two reference circular tubes is carried out, from $1.8d_o$ to $1.94d_o$ in steps of 1 mm, which implies an increment of the tubes separation.

Fig. 13 shows the maximum wall temperature, the mean tube temperature, the crown equivalent von Mises stress, and the thermal efficiency for the 5 cases analysed, including the reference circular tube (case $d_o$). In this occasion, the improvement of the mechanical behaviour of the receiver is noticeable while the thermal behaviour slightly improves. The stresses decrease from 476.6 MPa in the reference tube to 424.4 MPa for the case $1.8d_o$. In those cases, despite both the maximum and the mean tube temperature increase, the thermal efficiency increases around a 0.4% due to major internal convective coefficient of the HTF. Additionally, the increment of the temperature is not high enough to increase the corrosion problems in the receiver.

### 4.2.3. Optimisation comparison results

Table 2 summarizes the main results of this study, where the optimum oval configuration is the best in thermal efficiency terms, but is the worst referred to temperature and stress that would reduce the receiver lifetime. Ovoid geometry slightly improves all the aspects, but the improvements might not be enough to justify its use; while semicircles configuration improves both the efficiency and the stress, however this configuration penalizes the temperature, although it is still under the limiting corrosion temperature of the tube material in contact with molten salt. Thus, the last one is the optimal tube geometry selected in this study.

A more detailed analysis using FEM is carried out for the optimal geometry, the results show that the stress decreases from

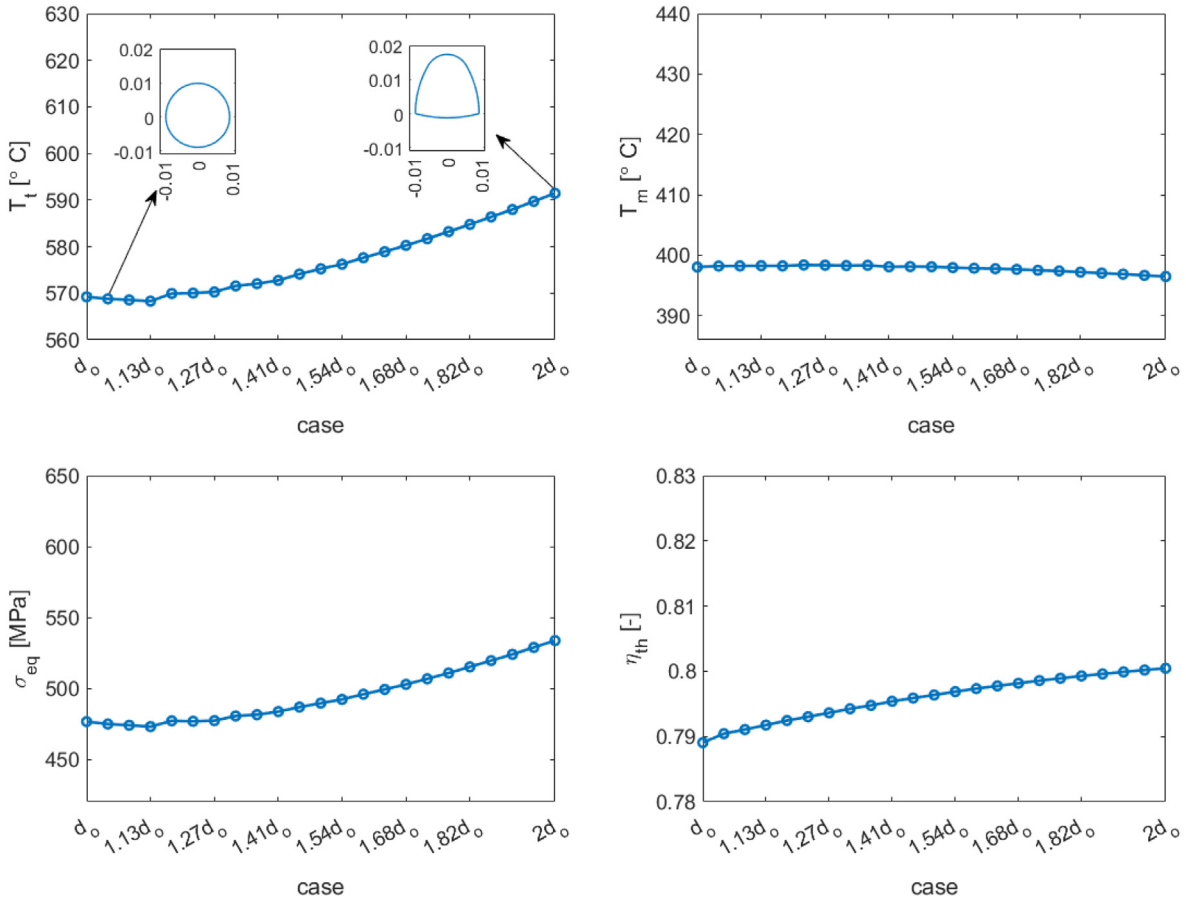


**Fig. 11.** Ovoidal cross-section tube results for the a) maximum tube wall, b) mean temperature of the tubes c) equivalent von Misses stress and d) thermal efficiency of the receiver for the most problematic axial division.

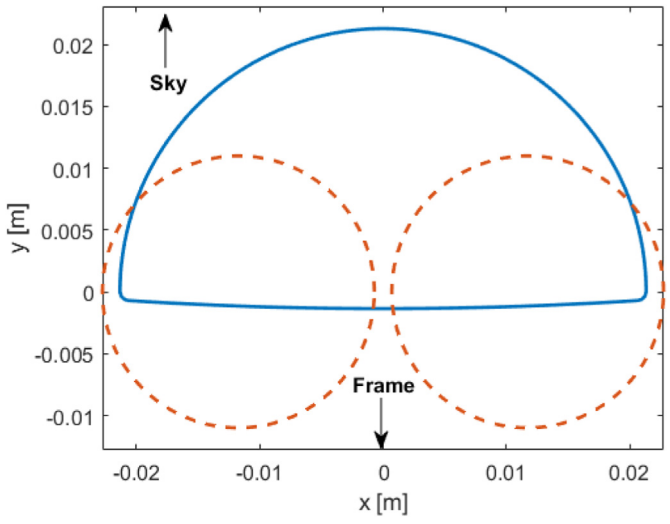


**Fig. 12.** Semicircle cross-section compared to the reference circular tube.

529.97 MPa in the circular reference tube to 477.52 MPa in the semicircle cross-section, which matches the 52 MPa predicted by the 1D model. Finally, a simulation of the whole receiver using the 2D mechanical model is depicted in Fig. 14, which shows the equivalent stress in the tube crown of all the axial divisions of each representative tube for the 9 panels that form a flow path of the receiver. The improvement of the stress occur in all the panels of the receiver, and not only in the most problematic axial section analysed previously.

Note that the assumption considered to analyse the stress is GPS, which is the most restrictive case for stress calculation. In real applications, where a finite number of supports is regarded, the displacements of the new tube geometries proposed could be even lower due to a major inertia moment, which would result in lower mechanical stresses.

### 4.3. Lifetime and cost analysis

Semicircle cross-section tubes are not only advantageous from a mechanical point of view, in which the stress reduction could increase the receiver useful life, but also this geometry reduces the costs of the receiver because the number of tubes, and the supports associated to them, are reduced by half. Supports are a critical point of the receiver, typically related to its failure. In this section, a lifetime and cost analysis for the reference receiver tube and the semicircle whose diameter is $1.8d_o$ is carried out to highlight the advantages that the new geometry can provide to SPT.

First, the damage model developed by Ref. [14] has been used to estimate the lifetime of both receivers. The model is fed with the elastic equivalent stresses ($\sigma_{eq}^{E}$) calculated with the 2D mechanical model. From these data the thermoplastic stresses ($\sigma_{eq}$) and deformations ($\Delta\varepsilon_{eq}$), as well as the stress relaxation ($\sigma_{relax}$) are calculated resulting in fatigue and creep damages ($d_f$ and $d_c$, respectively), which are added linearly to obtain the total lifetime

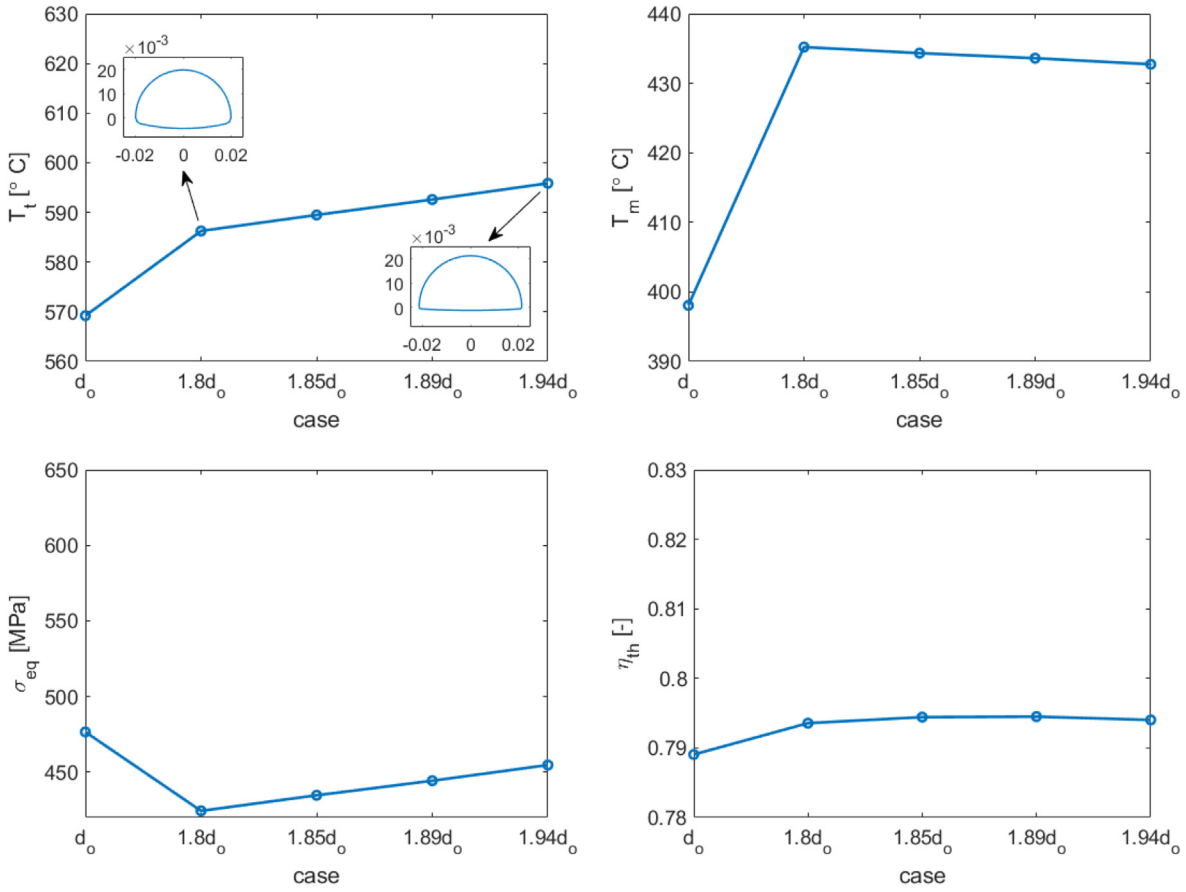


**Fig. 13.** Semicircle cross-section tube results for the a) maximum tube wall, b) mean temperature of the tubes c) equivalent von Misses stress and d) thermal efficiency of the receiver for the most problematic axial division.

**Table 2**
Temperature, equivalent stress (calculated with 1D model) and efficiency for the optimum tube geometry of each studied configuration.

| Configuration | Case | $T_{t,max}$ (°C) | Diff (%) | $\sigma_{eq,max}$ (MPa) | Diff (%) | $\eta_{th}$ (%) | Diff (%) |
|---|---|---|---|---|---|---|---|
| **Circular** | $d_o$ | 569.2 | – | 476.6 | – | 78.91 | – |
| **Oval** | $1.1d_o$ | 583.2 | −2.40 | 508.4 | −6.67 | 79.99 | **−1.37** |
| **Ovoid** | $1.13d_o$ | 568.3 | **0.15** | 473 | **0.75** | 79.18 | **−0.34** |
| **Semicircle** | $1.8d_o$ | 586.3 | −3.00 | 424.4 | **10.90** | 79.36 | **−0.57** |

in equivalent operating days (EODs).

$$EODs = \frac{1}{d_c + d_f} \tag{14}$$

$$d_c = \sum_{i=1}^{N} \frac{\Delta t_i}{t_{R,i}} \tag{15}$$

$$\log_{10}(t_R) = \beta_0 + \beta_1 \frac{1}{T} + \beta_2 \log_{10}(\sigma_{creep}) + \beta_3 \log_{10}(\sigma_{creep}) \frac{1}{T} \tag{16}$$

$$\sigma_{creep} = (\sigma_{eq} - \sigma_{relax}) / C' \tag{17}$$

$$\sigma^E_{eq}\varepsilon^E_{eq} = \frac{{\sigma_{eq}}^2}{E} + \sigma_{eq}\left(\frac{\sigma_{eq}}{K}\right)^{\frac{1}{n}} \tag{18}$$

$$\varepsilon^E_{eq} = \frac{\sqrt{2}}{3}\sqrt{\left(\varepsilon^E_r - \varepsilon^E_\theta\right)^2 + \left(\varepsilon^E_\theta - \varepsilon^E_z\right)^2 + \left(\varepsilon^E_z - \varepsilon^E_r\right)^2} \tag{19}$$

$$\sigma_{relax} = \sigma_{eq} - E\left[\left(\sigma_{eq}/E\right)^{1-n_r} - (1-n_r)AE^{n_r}\exp(-Q/(RT))\frac{t_{stab}^{m+1}}{m+1}\right]^{\frac{1}{1-n_r}} \tag{20}$$

$$d_f = \sum_{j=1}^{M} \frac{N_j}{N_{a,j}} \tag{21}$$

$$\frac{\Delta\varepsilon_{eq}}{2} = \frac{\Delta\varepsilon^E_{eq}}{2} = \frac{\sigma'_f}{E}N_a^{-c1} + \varepsilon'_f N_a^{-c_2} \tag{22}$$

The damage has been calculated in a conservative way, assuming that the receiver always works in the conditions of solar

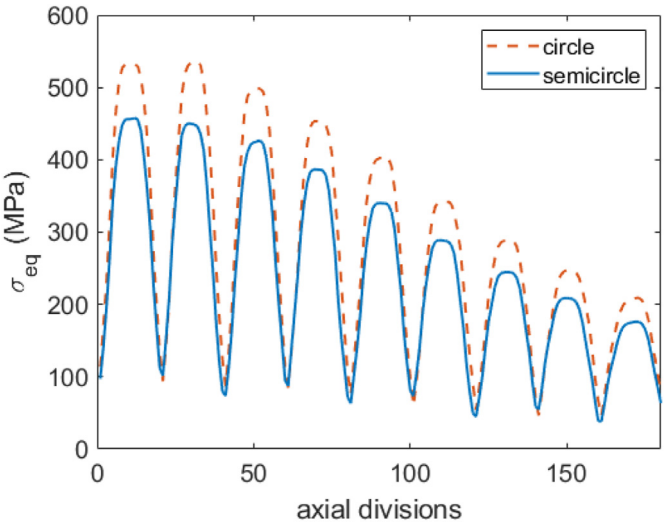


**Fig. 14.** Tube crown stress along the whole receiver calculated with the 2D model.

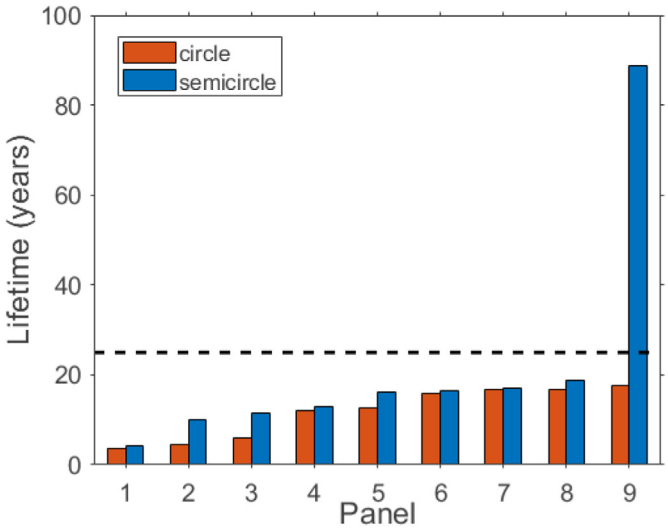


**Fig. 15.** Lifetime estimation of the panels of the receiver.

noon of the spring equinox, during an average of 7 h per day and 300 days per year, besides it is assumed that the equivalent stress never overpasses twice the elastic limit. Note that the lifetime estimation it is only valid for comparison purposes, but a more detailed analysis must be done for the final design of the receiver. Fig. 14 shows the lifetime of each of the 9 panels of a flow path for the reference circular tubes and the semicircle ones. The life of the circular tubes of all the panels is always lower than for the semicircle tubes, with significant relevance in the last panel of the flow path, in which the rupture time increases drastically due to its logaritmic relationship with the stress. Thus, for the typical 25 year-lifetime of an SPT plant and the information provided in Fig. 15 the number of replacements that each panel of the receiver requires can be obtained. Considering both flow paths of the receiver, a total of 44 panels must be replaced for the circular-tube receiver, opposite to the 30 substitutions that the semicircle-tube receiver demands for such same horizon.

Regarding the cost analysis, it has been taken into account the material price, 70 $/kg for Inconel 625 [29], which is involved in the manufacturing of receiver tubes and headers. Thus, to calculate the cost of the receiver material this price has been multiplied by the tube and headers volume, the material mean density for the working temperature range, 8440 kg/m$^3$, the number of tubes on each panel (64 for the reference circular tubes and 32 for the semicircle tubes) and the number of panels in the receiver (18) plus the number of panels substitutions required during the planned 25 years-lifetime of the plant. As the semicircular tube cannot be built in a traditional way, different techniques likeaditive manufacturing are required ans a correction factor has been included to the semicircular tube material cost that represents the manufacturing cost.

The cost of the initial application of Pyromark 2500 on the receiver tubes and the expected reapplications has been considered [30], being 287 $/m$^2$ and including an additional factor of 1.06 for the inflation from 2017 to 2020, and an annualized repaint cost of 11,050 $/year. On the other hand, each tube is connected to two nozzles and is welded to two headers and six clips. The cost of welding the tubes to clips and headers, the cost of the nozzles installation in each header, and the time required to install each conexion are available in Ref. [31], with the cost estimated to be of 65 $/man-hour, then using a 1.19 factor of inflation from the 2012 to 2021. The costs associated with having to shut down the plant to undertake the panels substitutions are omitted since, with the forecast of their expected lifetime, they can be scheduled during advance to take place in unfavourable operation conditions, such as a series of winter days.

$$C_{alloy} = (V_t N_t f + V_{hd} N_{hd})(N_p + N_{rep})\rho C_{625} \tag{23}$$

$$C_{coating} = [A_t N_t (N_p + N_{rep}) + C_{rp} N_{year}] C_{bp} \tag{24}$$

$$C_{specialties} = (N_t N_{hd,nz} t_{hd,nz} + N_{cp} t_{cp})(N_p + N_{rep}) C_{man} \tag{25}$$

Table 3 sumarizes the main parameters of the calculations:

As a result of all the above, a summary of the different aspects considered in the present costs analysis is shown in Table 4. The total cost of the circular-tube receiver is 7.9 M$, while the semicircular-tube receiver price is 45% lower when the tube manufacturing extra cost is not taken into account. Thus, the new receiver proposed would be economically feasible as long as the required manufacturing process does no overpass 3.5 times the current price of circular tube manufacturing.

## 5. Conclusions

To reduce the receiver failure, a series of asymmetrical cross-sections tubes have been analysed and compared with a reference circular cross-section tube by means of coupled thermal and mechanical models. For the conditions of study frontal oval tubes improve the thermal efficiency of the receiver up to 4%, but penalize the lifetime due to a relative increment of 12% in the equivalent stress. Ovoids penalize both the thermal and mechanical behaviour when the frontal part becomes peakier, while the thermal and mechanical variables remain almost constant when considering just small asymmetries. Finally, semicircle cross-sections tubes reduce the equivalent stress in the whole receiver, with a maximum reduction of a 9.9% with respect to the reference

**Table 3**
Cost parameters.

| Receiver | $A_t$ [m$^2$] | $V_t$ [m$^3$] | $V_{hd}$ [m$^3$] | $t_{nz\&nz}$ [h] | $t_c$ [h] | $f$ |
|---|---|---|---|---|---|---|
| Circle | 0.725 | 0.0011 | 0.002 | 3.5 | 2 | 1 |
| Semicircle | 1.1 | 0.0017 | 0.002 | 3.5 | 2 | 1 |

**Table 4**
Receiver costs.

| Alloy | Receiver | $C_{alloy}$ [$] | $C_{coating}$ [$] | $C_{specialties}$ [$] | $C_{tot}$ [$] |
|---|---|---|---|---|---|
| 625 | Circle | 2,756,673 | 1,168,813 | 3,990,022 | 7,915,509 |
| | Semicircle | 1,693,760 | 1,544,254 | 807,957 | 4,046,242 |

circular cross-section tubes, without compromising the thermal efficiency of the receiver.

Among these geometries, semicircle cross-section tubes give promising results. They reduce the stresses, increases the receiver lifetime, and reduce the number of tubes in the receiver and number of tube supports by half. This is economically favourable if the price of manufacturing the new tubes does not overpass 3.5 times the current price of circular tubes manufacturing. Hence, the use of semicircle cross-section tubes is strongly recommended in SPT tubular receivers.

## Credit Author

M.R. Rodríguez-Sánchez: Conceptualization, Methodology, Formal analysis, Writing – Original Draft, Editing, Funding acquisition, Project administration.

M Laporte-Azcué: Methodology, Software, Validation, Resources, Writing – Review & editing.

A. Montoya: Methodology, Software, Validation, Resources, Writing – Review &editing.

F. Hernández-Jiménez: Supervision, Methodology, Resources, Writing – Review & editing.

## Declaration of competing interest

The authors declare that they have no known competing financial interests or personal relationships that could have appeared to influence the work reported in this paper.

## Acknowledgements

This research is partially funded by the Spanish government under the project RTI2018-096664-B-C21 (MICINN/FEDER, UE) and by the Madrid Government (Comunidad de Madrid) under the Multiannual Agreement with UC3M in the line of "Fostering Young Doctors Research" (RETOrenovable-CM-UC3M), and in the context of the V PRICIT (Regional Programme of Research and Technological Innovation).

## References

[1] M. Mehos, H. Price, R. Cable, D. Kearney, B. Kelly, G. Kolb, F. Morse, Concentrating Solar Power Best Practices Study, National Renewable Energy Laboratory, Golden, CO, 2020. NREL/TP-5500-75763.
[2] O. Garbrecht, F. Al-Sibai, R. Kneer, K. Wieghardt, CFD-simulation of a new receiver design for a molten salt solar power tower, Sol. Energy 90 (2013) 94–106, https://doi.org/10.1016/j.solener.2012.12.007.
[3] W.Q. Wang, Y. Qiu, M.J. Li, F. Cao, Z. Bin Liu, Optical efficiency improvement of solar power tower by employing and optimizing novel fin-like receivers, Energy Convers. Manag. 184 (2019) 219–234, https://doi.org/10.1016/j.enconman.2018.12.029.
[4] C.K. Ho, Advances in central receivers for concentrating solar applications, Sol. Energy 152 (2017) 38–56, https://doi.org/10.1016/J.SOLENER.2017.03.048.
[5] G. Manzolini, G. Lucca, M. Binotti, G. Lozza, A two-step procedure for the selection of innovative high temperature heat transfer fluids in solar tower power plants, Renew. Energy 177 (2021) 807–822, https://doi.org/10.1016/J.RENENE.2021.05.153.
[6] X.L. Li, X.L. Xia, C. Sun, Z.H. Chen, Performance analysis on a volumetric solar receiver with an annular inner window, Renew. Energy 170 (2021) 487–499, https://doi.org/10.1016/J.RENENE.2021.01.141.
[7] Y. Chen, Y. Zhang, D. Wang, S. Hu, X. Huang, Effects of design parameters on fatigue–creep damage of tubular supercritical carbon dioxide power tower receivers, Renew. Energy 176 (2021) 520–532, https://doi.org/10.1016/J.RENENE.2021.05.069.
[8] M. Fernández-Torrijos, P.A. González-Gómez, C. Sobrino, D. Santana, Economic and thermo-mechanical design of tubular sCO2 central-receivers, Renew. Energy 177 (2021) 1087–1101, https://doi.org/10.1016/J.RENENE.2021.06.047.
[9] N. Boerema, G. Morrison, R. Taylor, G. Rosengarten, High temperature solar thermal central-receiver billboard design, Sol. Energy 97 (2013) 356–368, https://doi.org/10.1016/j.solener.2013.09.008.
[10] M.R. Rodríguez-Sánchez, A. Sánchez-González, D. Santana, Feasibility study of a new concept of solar external receiver: variable velocity receiver, Appl. Therm. Eng. 128 (2018) 335–344, https://doi.org/10.1016/J.APPLTHERMALENG.2017.08.173.
[11] J. Martinek, S. Jape, C.S. Turchi, Evaluation of external tubular configurations for a high-temperature chloride molten salt solar receiver operating above 700 °C, Sol. Energy 222 (2021) 115–128, https://doi.org/10.1016/j.solener.2021.04.054.
[12] S.M. Ismail, M.M. Rashwan, S. Ghani, Experimental and Numerical Investigation of Various Tube Geometries for Improved Heat Transfer in Solar Central Receivers, American Society of Mechanical Engineers, Fluids Engineering Division (Publication) FEDSM, Orlando (Florida), 2020, pp. 1–12, https://doi.org/10.1115/FEDSM2020-20139. FEDSM2020-20139.
[13] R. Pérez-Álvarez, M. Laporte-Azcué, A. Acosta-Iborra, D. Santana, Effect of eccentricity on the thermal stresses in a bayonet tube for solar power tower receivers, in: Solarpaces 2018: International Conference on Concentrating Solar Power and Chemical Energy Systems, 2019, https://doi.org/10.1063/1.5117553, 030041.
[14] P.A. González-Gómez, M.R. Rodríguez-Sánchez, M. Laporte-Azcué, D. Santana, Calculating molten-salt central-receiver lifetime under creep-fatigue damage, Sol. Energy 213 (2021) 180–197, https://doi.org/10.1016/j.solener.2020.11.033.
[15] A. Sánchez-González, M.R. Rodríguez-Sánchez, D. Santana, Aiming factor to flatten the flux distribution on cylindrical receivers, Energy 153 (2018) 113–125, https://doi.org/10.1016/j.energy.2018.04.002.
[16] A. Sánchez-González, C. Caliot, A. Ferrière, D. Santana, Determination of heliostat canting errors via deterministic optimization, Sol. Energy 150 (2017) 136–146, https://doi.org/10.1016/J.SOLENER.2017.04.039.
[17] A. Sánchez-González, D. Santana, Solar flux distribution on central receivers: a projection method from analytic function, Renew. Energy 74 (2015) 576–587.
[18] M.R. Rodríguez-Sánchez, A. Soria-Verdugo, J.A. Almendros-Ibáñez, A. Acosta-Iborra, D. Santana, Thermal design guidelines of solar power towers, Appl. Therm. Eng. 63 (2014b) 428–438, https://doi.org/10.1016/j.applthermaleng.2013.11.014.
[19] M.R. Rodríguez-Sánchez, C. Marugan-Cruz, A. Acosta-Iborra, D. Santana, Comparison of simplified heat transfer models and CFD simulations for molten salt external receiver, Appl. Therm. Eng. 73 (2014a) 991–1003, https://doi.org/10.1016/j.applthermaleng.2014.08.072.
[20] F.M. Modest, Radiative heat transfer, in: Radiative Heat Transfer, Elsevier science, New York, San Francisco, London, 2003, pp. 162–197.
[21] Babcock, Wilcox Company, Molten Salt Receiver Subsystem Research Experiment Phase 1 - Final Report, ume 1 – Technical, Barberton, Ohio, 1984.
[22] M. Laporte-Azcué, P.A. González-Gómez, M.R. Rodríguez-Sánchez, D. Santana, Deflection and stresses in solar central receivers, Sol. Energy 195 (2020) 355–368, https://doi.org/10.1016/J.SOLENER.2019.11.066.
[23] A. Montoya, M.R. Rodríguez-Sánchez, J. López-Puente, D. Santana, Influence of longitudinal clips in thermal stresses and deflection in solar tubular receivers, Sol. Energy 198 (2020), https://doi.org/10.1016/j.solener.2020.01.030.
[24] S.P. Timoshenko, J.N. Goodier, Theory of Elasticity, I. ed., McGraw-Hill, New York, 1951.
[25] A.B. Zavoico, Solar Power Tower: Design Basis Document, 2001. San Francisco, SAND2001-2100.
[26] J.I. Burgaleta, S. Arias, D. Ramirez, Gemasolar, the first tower thermosolar commercial plant with molten salt storage, in: Solarpaces, 2011, pp. 1–8.
[27] American Society of Mechanical Engineers, ASME Boiler and Pressure Vessel Code II, Part D: Properties (Metric) Materials, 2010. New York, USA.
[28] C.K. Ho, A. Roderick Mahoney, A. Ambrosini, M. Bencomo, A. Hall, T.N. Lambert, Characterization of Pyromark 2500 paint for high-temperature solar receivers, J. Sol. Energy Eng. 136 (2013) 4, https://doi.org/10.1115/1.4024031.
[29] M. Laporte-Azcué, P.A. González-Gómez, M.R. Rodríguez-Sánchez, D. Santana, Material selection for solar central receiver tubes, Sol. Energy Mater. Sol. Cells 231 (2021) 111317, https://doi.org/10.1016/J.SOLMAT.2021.111317.
[30] A. Boubault, C.K. Ho, A. Hall, T.N. Lambert, A. Ambrosini, Durability of solar absorber coatings and their cost-effectiveness, Sol. Energy Mater. Sol. Cells 166 (2017) 176–184, https://doi.org/10.1016/j.solmat.2017.03.010.
[31] B. Kelly, M. Izygon, L. Vant-Hull, Advanced Thermal Energy Storage for Central Receivers with Supercritical Coolants, Lakewood, CO, 2010, https://doi.org/10.2172/981926.